

9-9-1987

Advanced Scanning Electron Microscopy Methods and Applications to Integrated Circuit Failure Analysis

E. I. Cole Jr.

University of North Carolina at Chapel Hill

C. R. Bagnell Jr.

University of North Carolina at Chapel Hill

B. G. Davies

University of North Carolina at Chapel Hill

A. M. Neacsu

University of North Carolina at Chapel Hill

W. V. Oxford

University of North Carolina at Chapel Hill

See next page for additional authors

Follow this and additional works at: <https://digitalcommons.usu.edu/microscopy>



Part of the [Biology Commons](#)

Recommended Citation

Cole, E. I. Jr.; Bagnell, C. R. Jr.; Davies, B. G.; Neacsu, A. M.; Oxford, W. V.; and Propst, R. H. (1987) "Advanced Scanning Electron Microscopy Methods and Applications to Integrated Circuit Failure Analysis," *Scanning Microscopy*: Vol. 2 : No. 1 , Article 14.

Available at: <https://digitalcommons.usu.edu/microscopy/vol2/iss1/14>

This Article is brought to you for free and open access by the Western Dairy Center at DigitalCommons@USU. It has been accepted for inclusion in Scanning Microscopy by an authorized administrator of DigitalCommons@USU. For more information, please contact digitalcommons@usu.edu.



Advanced Scanning Electron Microscopy Methods and Applications to Integrated Circuit Failure Analysis

Authors

E. I. Cole Jr., C. R. Bagnell Jr., B. G. Davies, A. M. Neacsu, W. V. Oxford, and R. H. Propst

Advanced Scanning Electron Microscopy Methods and Applications to Integrated Circuit Failure Analysis

E.I.Cole Jr.¹, C.R. Bagnell Jr.², B.G. Davies³, A.M. Neacsu¹, W.V. Oxford³, R.H. Propst^{1,3}

¹Department of Physics,

²Department of Pathology,

³Biomedical Engineering,

University of North Carolina at Chapel Hill

Chapel Hill, North Carolina 27514

(Received for publication November 09, 1986, and in revised form September 09, 1987)

Abstract

Semiconductor device failure analysis using the scanning electron microscope (SEM) has become a standard component of integrated circuit fabrication. Improvements in SEM capabilities and in digital imaging and processing have advanced standard acquisition modes and have promoted new failure analysis methods. The physical basis of various data acquisition modes, both standard and new, and their implementation on a computer controlled SEM image acquisition/processing system are discussed, emphasizing the advantages of each method. Design considerations for an integrated, on-line failure analysis system are also described. Recent developments in the integration of the information provided by electron beam analysis, conventional integrated circuit (IC) testing, computer-aided design (CAD), and device parameter testing into a single system promise to provide powerful future tools for failure analysis.

KEYWORDS: Failure analysis, voltage contrast, capacitive coupling voltage contrast, electron beam induced current, resistive contrast imaging, backscattered electron imaging, digital image processing.

Address for correspondence:

R.H. Propst

Biomedical Engineering

University of North Carolina at Chapel Hill

Chapel Hill, North Carolina 27514

Phone No. (919) 966-4578

Introduction

The scanning electron microscope is a unique tool for the failure analysis of semiconductor devices in that it can provide a wide variety of functional as well as physical information simultaneously using different imaging modes. Each SEM data acquisition mode offers different advantages for given applications. Voltage contrast (VC) imaging can provide accurate voltage measurements on the device under test (DUT), but VC accuracy is limited by system noise and drift, and is of limited use for passivated devices. VC measurement reliability can be enhanced by using referenced voltage levels for calibration on the DUT. Electron beam induced current (EBIC) imaging is useful for locating p-n junctions. This technique has the useful property that it functions well even on passivated devices. However, with a primary beam energy of several keV (which is required to generate a useful EBIC current), damage to MOS (metal-oxide-semiconductor) device structures can occur.

The resistive contrast imaging (RCI) technique is similar to EBIC. The hardware is identical, however, for RCI the signal current is not generated by the separation of electron-hole pairs in the junction region. The RCI method uses the current flow between two reference nodes, generated by the incident primary beam to produce an image. The image intensity is proportional to the ratio of the path resistance from the primary beam impact point to these two points. RCI is very useful for characterizing bulk resistance in materials as well as for locating open and short-circuited paths on devices. Capacitive-coupling voltage contrast (CCVC) imaging depends on the "coupling" of dynamic subsurface voltage transients below an oxide or passivation layer to a visible surface layer. Because the primary beam need not penetrate through the insulating upper layer, low primary beam voltages may be used. This method allows the observation of voltage levels on devices

below a passivation layer, which is of great interest as devices become more vertically integrated. CCVC can be understood when viewed as a parallel plate capacitor whose bottom plate is formed by the application of an unknown voltage to a subsurface structure, a passivation layer as the dielectric, and a top plate created by the conductive surface layer induced by the primary SEM beam. The primary e-beam will discharge the capacitor in a time proportional to the incident current flux. Two methods have been developed for quantitative voltage measurement of subsurface levels using CCVC: energy spectrometry, which requires the installation of non-standard SEM hardware, and Time Resolved Capacitive Coupling Voltage Contrast (TRCCVC), described below.

Another necessary ingredient in the SEM failure analysis of integrated circuits is the knowledge of subsurface layer geometry. This is important for two reasons: 1) to enable mask alignment validation to be performed by the SEM, and 2) to enable the identification of faults (such as broken metallization). Backscatter Electron (BSE) imaging as well as TRCCVC have shown initial promise in this area.

Finally, digital signal processing, noise analysis, and image enhancement are indispensable tools for augmenting each of the techniques discussed above and further development in this area is necessary for the implementation of an automated SEM analysis system. The following will discuss the elements outlined above, as well as their integration into a complete SEM failure analysis system.

Voltage Contrast

For secondary electron imaging, the image intensity is dependent on the number of secondary electrons collected as the primary electron beam is scanned across the sample. Voltage contrast (VC) imaging is the phenomenon observed when differences in potential on the SEM sample produce image intensity modulation. VC imaging was demonstrated as early as 1935 [18]. In 1974, Wells classified contributions to the VC signal into two categories: local field contrast and collector contrast [44]. He also discussed some of the difficulties encountered in making quantitative voltage measurements from the secondary electron signal.

In local field contrast, the image modulation results from a reduction in the low-energy secondary electron emission from areas on the device with a positive potential. These potential differences may be produced by the application of voltages to the DUT from an external source. Collector contrast is the modulation of the secondary electron signal observed at the detector and is produced by

non-uniform secondary collection characteristics. These non-uniformities can result from non-symmetric collector geometries with respect to the DUT or from energy-dependent selection of the secondary electrons by the collector. Thus, a distinction is made between the total secondary current produced by the primary beam interactions with the sample and that fraction of the total which is collected by the SE detector. A wider definition of collector contrast should also include contributions to the image by the noise and drift present in the detector hardware. The determination of the absolute voltage present on an arbitrary DUT, however, is primarily dependent on those contributions which are due to local field contrast. Since all secondary collectors exhibit some degree of collector contrast, many techniques for analyzing and reducing this contribution to the overall VC signal have been examined. Various methods which exploit different combinations of non-standard collector geometries [8], secondary electron extraction grids, and energy selection of the secondary electrons [10] are used to measure an absolute (non-referenced) voltage.

There are at least three different methods of determining the absolute voltage present on a given device using the secondary electron signal. The first method involves the analytical modeling of the voltage contrast phenomenon (incorporating the many contributions to the secondary electron current, such as collector geometry contrast, atomic number contrast, secondary energy distribution, etc..) and determining the ideal secondary electron current for various voltages at different locations on the DUT. This technique is extremely difficult to implement because there are so many factors which interact to produce the voltage contrast phenomenon.

Another possible method is to use a properly operating "reference" device and simply compare the differences in the voltage contrast signal between the two devices, rather than trying to perform the voltage-contrast by absolute voltage mapping. If the absolute voltage difference between the two devices is needed, however, both voltage contrast measurements must be converted into voltage before comparing the two voltage levels. However, for a large portion of IC failure analysis work, the simple fact that a voltage anomaly exists at a certain point in the circuit is enough information. Admittedly, this "voltage referencing" procedure is not without problems (the most obvious of which is the correct alignment of the two different test devices), but it is a simpler process by far than the determination of absolute voltage levels on the two devices.

Another method to determine the voltage present at a given location on the DUT is to compare the secondary signal from the "powered-up" device with

the signal when the same device is at ground potential. This method of performing a "relative" voltage contrast determination is a much easier task, since all that is needed is an image of the device where every input has been grounded and an image of the same device with voltage applied. In this manner, the voltage contrast information can be isolated from the topographical and collector contrast signal components (discussed below) by image subtraction or some other suitable processing technique. The only remaining task is then to map this voltage contrast intensity change into absolute voltage change. However, the noise and drift components of collector contrast cannot be reduced as easily as the other components and for this reason, image data processing of some kind is necessary. This procedure has also been discussed at length in the literature [7].

Thus, absolute voltage determination is not a necessity in order to adequately assess the operation of the DUT for most failure analysis applications. In those cases where the absolute voltage is required, a number of commercial "E-beam testers" are available. However, these systems are generally dedicated units and lack the flexibility to perform many of the more useful techniques (such as EBIC imaging) provided by the standard SEM. In addition, for most production semiconductor devices, a correctly operating standard is available for comparison purposes.

Improving VC Resolution

In 1974, Wells reported the absolute limit of voltage contrast resolution to be on the order of 1.0 volt for a non-referenced voltage system [44]. An SEM IC analysis system which was constructed completely from standard off-the-shelf parts produced VC resolutions of around 40 mV for direct waveform measurements and 400 mV for images in 1981 [4]. By 1985, a system with a 25 mV VC resolution and a 0.1 ns temporal resolution had been described [29]. However, a stroboscopic data acquisition system was required to achieve this performance. Since stroboscopic methods significantly reduce the number of secondary electrons which reach the detector, a large primary beam current was needed to produce an acceptable SNR. When combined with the accelerating voltage of about 1.0 keV necessary to prevent damage to an MOS structure, the primary beam spot size limited spatial resolution to a feature width of greater than 4 microns. This is obviously unacceptable for present-day VLSI devices which exhibit minimum feature sizes on the order of 1 micron. By reducing the primary beam spot size a minimum feature size of 2 microns was achieved, but with a corresponding reduction in VC resolution to roughly 50 mV.

Theoretical calculations of the maximum available voltage resolution for a given set of microscope operating parameters have been presented for both static [42] and stroboscopic [1] VC systems. In 1986, a method of calculating this theoretical limit for an electron energy spectrometer detector using a secondary electron extraction grid arrangement was demonstrated [6]. This method used finite element analysis techniques to calculate the trajectories of typical secondary electrons and the electric field produced by the extraction grid-detector arrangement. With these results, the optimum operating points for each of the elements in the secondary detection system could be calculated, allowing the system to be adjusted for the minimum amount of collector contrast. However, one problem with this system (and for any system which utilizes a secondary electron extraction grid), is the limited field-of-view. IC die sizes can extend up to 1 cm on a side and the physical dimensions of the extraction grid can limit the scanning field to somewhere on the order of 20 microns on a side. Thus, the stage must be moved using stepper motors in order to examine the entire die. This slows down the data acquisition process and increases the possibility of inaccuracies in beam positioning. Another disadvantage of this and other techniques which employ non-standard hardware (such as the extraction grid or the secondary electron spectrometer) is limited availability and major SEM column modifications for installation.

Data processing of the digitized secondary electron signal offers an additional method for increasing VC resolution and accuracy. Subtraction of the secondary signal which contains voltage contrast information from one which does not has been shown to increase VC linearity [11]. This method is based on the premise that the voltage contrast signal is actually a linear combination of a number of components, one of which is directly related to the voltage present on the DUT. With all other parameters held constant, the voltage-dependent component can be isolated by subtracting two images in which the voltage present on the DUT has been changed. The processing techniques used to improve VC linearity have typically been limited to simple subtraction of one image frame from another. However, other processing methods have proven more effective. In 1986, DiBianca et al. reported voltage errors on the order of 25 mV without the use of non-standard secondary detector hardware or stroboscopic acquisition techniques [7]. This resolution was achieved by applying least-squares fitting to known voltage references on the same device as the node to be tested, referencing the unknown VC data to the fitted reference data.

Another class of VC data isolation methods are dynamic VC techniques [5,23]. These techniques are useful for two main reasons. First, static voltage contrast methods are nearly useless for passivated MOS devices, since the low primary beam energies required to prevent the generation of X-rays (which may damage the DUT) cannot penetrate the passivation layer (see Capacitive Coupling Voltage Contrast below). Second, some IC failure modes are inherently dynamic in nature. Such faults appear as the device is cycled at a rate which exceeds its maximum speed of operation. In the time required to acquire a typical single VC image, a dynamic fault may have propagated through several hundred gates in a given circuit, making it impossible to determine the transistor in which the fault occurred. In order to isolate the malfunctioning device, the chip is repeatedly cycled through the set of states in which the fault occurs. A beam blanker (with a duty cycle on the order of 1 nanosecond) is then used to turn the primary electron beam on and off synchronously with the DUT cycle. The stroboscopic VC data is digitized by sampling the secondary signal with a video-rate frame grabber and storing the result in a frame buffer.

Image Noise Analysis

Noise in SEM images can be attributed to two primary sources: 1) thermal/random system noise, and 2) quantization noise during A/D conversion [32]. Much work has been done in the noise analysis field to develop models which will characterize noise and suggest methods to mitigate noise. Some general results from noise analysis have had particularly successful application in SEM image processing.

The linear noise model widely used in systems and information theory is based upon the notion of stochastic processes, such as Poisson, Gaussian, or Markov, and the associated probabilistic description of events. In this sense, noise is defined as a random fluctuation in the record of a signal. This description has successfully yielded a host of powerful tools to measure and quantify as well as to minimize noise. A partial litany of established image processing tools includes: (i) low-pass filtration [32] of SEM image signals that reduces high-frequency signature components of noise, (ii) a related, but slightly different procedure--mean pixel value substitution, (iii) non-linear or "thresholded" subtraction [31], and (iv) Fourier Transform filtering. In addition to these techniques which operate on a single image, frame averaging, wherein a multiplicity of images from the SEM are averaged, has been implemented widely. Some examples of the results of frame averaging and fast

Fourier Transform analysis are shown in Figures 1-4.

In addition to the linear models of noise and their related methods of suppression, there are non-linear models which may offer new approaches to the enhancement of signal-to-noise ratios. One of the goals of current research in this field is to develop new models to characterize noise [31].

Capacitive Coupling Voltage Contrast

Problems encountered when using an SEM in the VC mode on passivated devices have been well documented [14,38,19,39,43]. To minimize the damage to non-radiation hardened MOS devices by the primary electrons or the X-rays generated by these electrons, low primary electron beam energies (< 1.0 keV) or special scanning methods such as windowing must be used [14]. Since low energy primary electrons penetrate only into the uppermost portion of the passivation layer, no static voltage contrast is visible [24]. However, a change in potential on a subsurface structure will polarize the insulating material between the structure and the surface (Figure 5). The bound surface charge associated with this polarization produces a transient increase or decrease in the secondary electron signal. This signal can be used to generate a dynamic VC image - capacitive coupling voltage contrast (CCVC) (Figure 6).

Physical Basis of Signal Generation

A primary electron beam incident on a solid will cascade into many excited electrons by collisions as it travels through the material. These excited electrons lose energy through elastic as well as inelastic scattering processes. However, some retain sufficient excitation to escape from the solid at the surface. Secondary electrons (SE) are, by definition, electrons with energy ≤ 50 eV which escape the surface. The shape of the SE energy distribution for primary electron beams of energy >100 eV is determined by the work function, Fermi level, and other parameters of the material under investigation [35]. If the loss current (I') does not equal the primary beam current (I_{PE}), there will be a net charge accumulation on the device. At the beam energies used for CCVC, there are two major sources of I' : SE and BSE [13]. The backscattered electrons are the electrons emitted from the sample which have undergone primarily elastic scattering events. The ratio (η), of BSE current to I_{PE} (defined by I_{BSE}/I_{PE}) is a constant, independent of beam energy for incident beam energies greater than about 5 keV [32]. At lower energies, η becomes energy dependent. The ratio (δ), of SE current to the primary beam current (defined by I_{SE}/I_{PE}) depends upon the sample material as well as

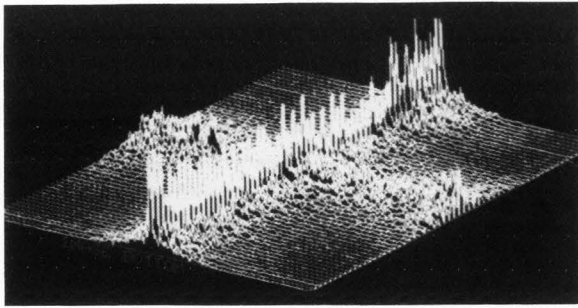


Figure 1. Two dimensional Fourier Transform of noisy video image [31].

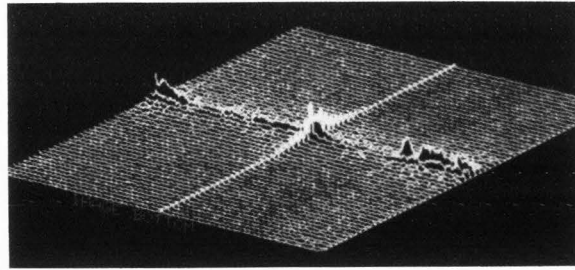


Figure 2. Two dimensional Fourier Transform of video image with enhanced signal-to-noise ratio [31].

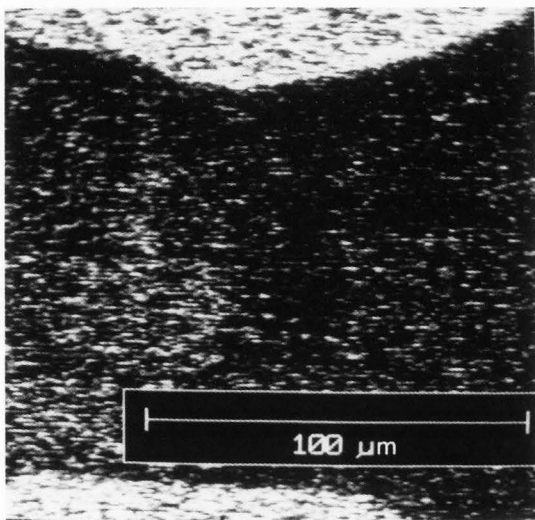


Figure 3. Single video frame SEM image [31].

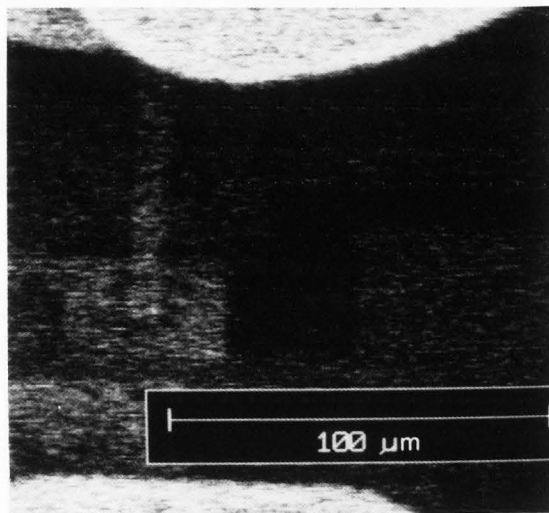


Figure 4. Average of 8 video frames for SEM image [31].

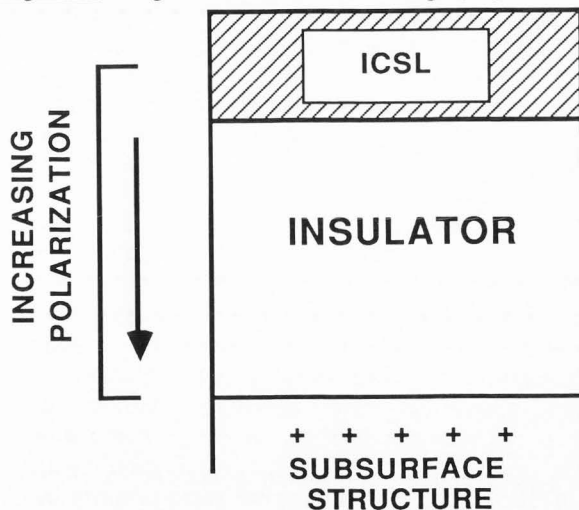


Figure 5. Polarization of the insulating passivation between the induced conductive surface layer (ICSL) and a subsurface structure caused by a voltage transition [31].

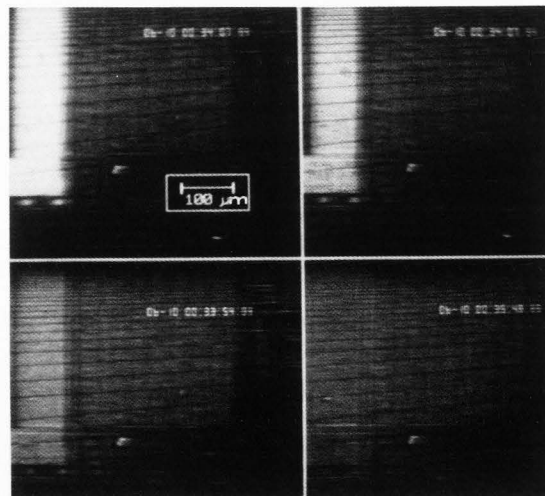


Figure 6. SE images at 1.25 keV primary beam energy at 0, 1, 2, and 3 seconds after a 3 volt transition [31].

the energy of the primary beam [35]. If the sum of the

BSE and SE currents exceed I_{PE} (as is the case for CCVC), a net positive charge will build up on the surface. This charge prevents lower energy SE's from escaping the surface and decreases the intensity of the SE image. An equilibrium voltage is reached when the net charge accumulated on the device does not change with time. A bound surface charge will be produced when structures below the maximum beam penetration depth change potential, and material between them and the surface becomes polarized. The CCVC signal is the change in the number of SE's caused by this bound charge potential, which decays back to the equilibrium potential as SE's escape.

Experimental and Modeling Results

Quantitative voltage measurements using capacitive coupling voltage contrast have been achieved by two different methods: 1) retarding field spectrometry and 2) Time Resolved Capacitive Coupling Voltage Contrast (TRCCVC) [12,5]. The methods exploit different properties of the same physical phenomena. Each has its advantages and disadvantages and the methods tend to complement each other.

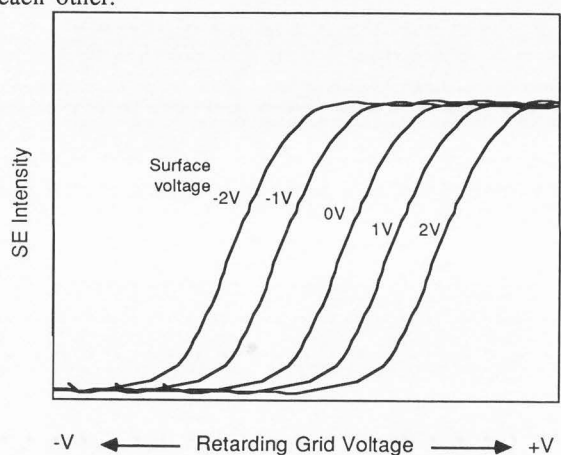


Figure 7. S-shaped curves generated by field spectrometry [12].

Fujioka et al. have demonstrated field spectrometry on passivated electrodes [12]. In this technique, the area to be examined is scanned for several minutes until the surface reaches equilibrium.

Next, a retarding grid with variable voltage (-10 to +10 V) is placed over the test device (the beam is in spot mode). Immediately after a voltage change, the secondary electron signal is measured with respect to the retarding grid voltage. The varying grid voltage produces the S-shaped curves seen in Figure 7. A least squares fit of the retarding grid voltage (V_r) vs the applied voltage (V_s) for half the maximum SE intensity yields a linear calibration

curve. Fujioka et al. reported standard errors of 30 to 140 mV for various samples and voltage ranges. They have also reported the application of this technique to nonpassivated structures, with similar results.

This method requires that the effects of the bound charge on the local electric field are measured before the primary electron beam has had time to change the bound surface charge significantly. The time necessary to perform a single voltage measurement is 14 msec. For the beam energy and current used (1 keV and 10 pA), the bound charge is presumed to be constant over the measurement period. This is in contrast to the TRCCVC method, which takes advantage of the time dependency of the bound charge to measure voltage.

By operating the SEM at a standard video rate, dynamic SE image data can be analyzed on-line or videotaped for later examination on an image processing system. In this technique, the voltages applied to the DUT are square waves with variable period and amplitude. All periods are long enough to allow complete decay of the voltage contrast flash in the secondary electron image. Image contrast decay data can be obtained using a video-rate digitizer. The digitizer converts the analog composite video signal into a digital image. Because it is based on a standard video format, the resulting system has a minimum sampling period of 33.3 msec (video rate of 30 frames per second).

Since the decay time of a given voltage contrast flash is inversely proportional to the incident flux of the SEM primary beam, the primary electron beam current must be carefully chosen [5]. The transient decay times must be long relative to the system sampling rate. The low flux required for adequate time resolution results in a poor signal-to-noise ratio (SNR) for the SE image. To increase the SNR, multiple frames of the voltage contrast flash, synchronous in time with the applied square wave, are averaged. The voltage contrast amplitude in the averaged SE image is then determined as a function of time.

For sufficiently large negative voltage transients, a "saturation effect" of the dynamic voltage contrast signal occurs. The amplitude of the dynamic voltage contrast flash (and therefore the number of SE's leaving the device surface) is constant for a certain time after the transition. The saturation parameters depend upon the SEM operating conditions as well as the work function and the energy distribution of the excited electrons in the passivation layer. Larger voltage shifts saturate at the same intensity but remain saturated for a longer time interval.

The monotonic relationship between saturation time and the amplitude of the negative voltage shift is used to make a voltage calibration curve [5].

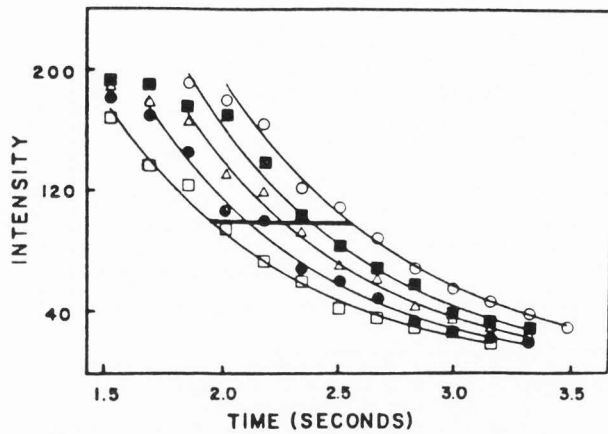


Figure 8. Measured decay data and best fit exponential curves for -4.0 to -5.0 volts applied transients, left to right, in 250 mV steps. The line across the plot is the target intensity value [5].

Using multiple frame averaging, the decay data for different voltage level transients can be plotted (Figure 8). Following Menzel and Kubalek's suggestion [24] that the voltage contrast flash should decay exponentially (modeled on a simple parallel plate capacitor), a least-mean-squares fit of the decay data (intensity vs. time) to an exponential curve can then be calculated. The result is a series of exponential curves, each representing the decay of a given voltage level. The decay time required by any given flash to reach a fixed target intensity is then used to quantify the amplitude of the voltage pulse. The TRCCVC method has been evaluated using an npn power transistor and a Schottky diode, both passivated. The experimental conditions and results are shown in Table 1 [5]. As reported by Cole et al. the data collection for the calibration curves of Table 1 required an hour. Recent software modifications have reduced this time to 8 minutes [31]. All of the capacitive coupling data presented was acquired with the primary electron beam perpendicular to the sample. The secondary collector was 3 centimeters from the sample, about 10 degrees above the plane of the device. The collector cage was held at 300 volts. For transitions over the 1-5 V range the maximum standard error is 106 mV. However, over 1 volt intervals the error varies from 16mV to a maximum of 45 mV. These resolutions compare with or surpass those published using retarding field spectrometry [12]. Quantitative voltage measurement without referencing requires modeling of the CCVC decay. In order to predict the shape of the SE decay curves, the SE energy distribution, surface equilibrium voltage, and incident electron flux must be known. Gorlich et al. [13] suggest using closed form equations for the SE energy distribution, (Eq. 1),

Table 1. Experimental conditions and voltage resolutions using the time-resolved capacitive coupling voltage contrast technique on two different devices [5].

Device	Primary beam energy (kV)	Sample area (pixels ²)	Frames averaged	Voltage range (V)	Standard error (mV)
Diode	2.50	64x64	14	1-5	58.5
Diode	2.50	64x64	10	0.75-2.75	28.5
Transistor	1.25	32x64	5	1-5	106.1
Transistor	1.25	32x64	5	0.75-2.00	44.8
Transistor	1.25	32x64	5	2-3	44.3
Transistor	1.25	32x64	5	3-4	34.6
Transistor	1.25	32x64	5	4-5	16.3

for the SE energy distribution, (Eq. 1), and for δ , (Eq. 2) [34,35].

$$N = \frac{E_{SE}}{(E_{SE} + A)(E_{SE} + \Phi)^\gamma} \quad (1)$$

where E_{SE} = the secondary electron energy, N = the number of SE at energy E_{SE} , and A , Φ , and γ are empirically determined constants. The values used for the constants were as follows: $\Phi = 5$ eV (approximating the work function for SiO_2), $A = 0.35$ eV and $\gamma = 2$.

$$\delta = (Q)^{0.38} 1.11 \delta_{\max} (1 - e^{-2.3Z}) \quad (2)$$

where $Q = E_{PE} / E_{PE\max}$, $z = Q^{1.35}$, E_{PE} = primary beam energy, and $\delta = I_{SE} / I_{PE}$ (δ_{\max} refers to the maximum value for δ). In addition, the time dependent potential on the surface, $V(t)$, is predicted to decay like that across a capacitor in an RC circuit, i.e.,

$$V(t) = \frac{d}{A\epsilon_0} \int_0^t I_{AE}(t') dt' \quad (3)$$

where $V(t)$ = the surface voltage at time t , ϵ = the permittivity of the passivation, A = the area scanned, $I_{AE} = I_{SE} + I_{BSE} - I_{PE}$, and d = the structure depth. The net absorbed current, I_{AE} , will be a function of the number of SE's with energies greater than that of the surface potential:

$$I_{AE}(E') = \left[\frac{\delta \int_0^E N(E') dE'}{50} + \eta - 1.0 \right] I_{PE} \quad (4)$$

where $\eta = I_{BSE}/I_{PE}$ and E is the potential energy at the surface from charge buildup. It is obvious that even with Eqs. 1 and 4, $V(t)$ cannot be solved in closed form. An iterative solution can be formulated assuming that $V(t = 0)$ is known:

$$V(t + \tau) = V(t) + \tau \left(\frac{d}{AE} \right) I_{AE}(E)V(t) \quad (5)$$

where τ = some small time interval and $E = V(t)$ is the surface potential from charge buildup at time t . Applying constants for SiO_2 [13,34] and typical SEM and device parameters to the above equations, $V(t)$ can be solved as shown in Figure 9. Qualitatively, the curves exhibit the same general shape recorded earlier (including the "saturation" region). However, the curves in Figure 9 do not agree with experimental results. There are several reasons for the differences. First, the expression for the SE energy distribution (Eq 1.) does not include the effects of the surface contaminants, which build with exposure. These contaminants are crosslinked hydrocarbon chains which can significantly alter the SE emission efficiency [15]. Second, the value of $V(t = 0)$ for a given transient on a subsurface structure will be a function of surface contaminants and incident beam energy as well as the amplitude of the voltage change. Third, the value for η and the expression for δ do not fit the experimental data well at low primary beam energies. Reimer has shown that η may change a great deal below 5 keV [32]. Additionally, the values of δ_{\max} for SiO_2 vary between 2.1 and 2.9 depending on the processing [35].

To compare experimental results with those predicted by the model presented above, the integral SE distribution can be measured from the CCVC signal. To understand how this information is measured, consider Figure 10, which shows an arbitrary SE energy spectrum for a given material. The horizontal axis is the energy of the SE's and the vertical axis is the number of SE's at a particular energy. If the integral of this curve is normalized, the

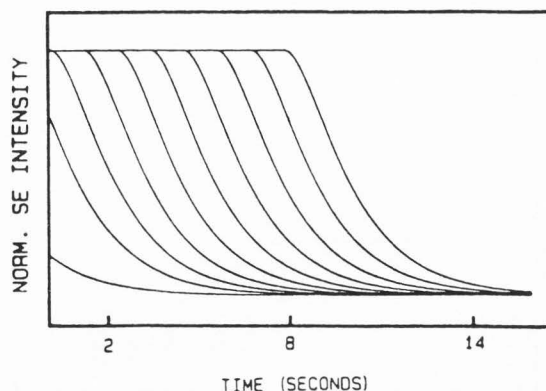


Figure 9. Calculated CCVC decay curves from 0.4 to -1.4 volts initial surface voltage, 0.2 volt steps, using modeled SE energy distributions [31].

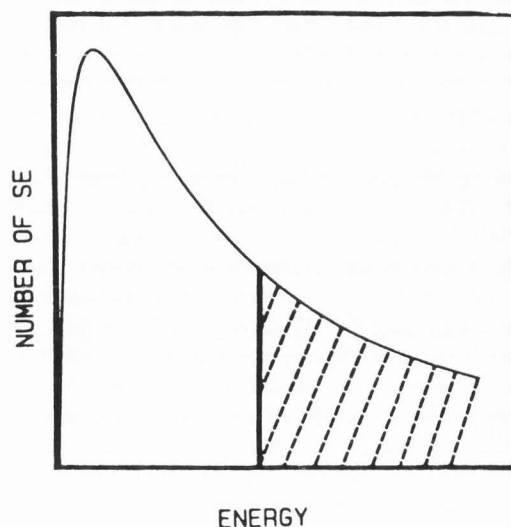


Figure 10. Arbitrary SE energy distribution.

resulting curve could be considered the probability of finding SE's at a given energy. When an SE image is produced from a surface at a particular potential, all of the electrons with energies greater than the potential of the surface will escape (the shaded region of Figure 10). The intensity of the image will be proportional to the integral from the applied potential to infinity of the probability distribution. (Conventionally, the upper limit of the integral is 50 eV for SE's.) Thus, for the number of SE's or intensity of an image, $I(V)$,

$$I(V) = \int_V^{50} \rho(V') dV' \quad (6)$$

Immediately after an applied transition voltage the surface potential equals the sum of the applied voltage and the potential of the surface before the transition. The CCVC contrast is the integral SE

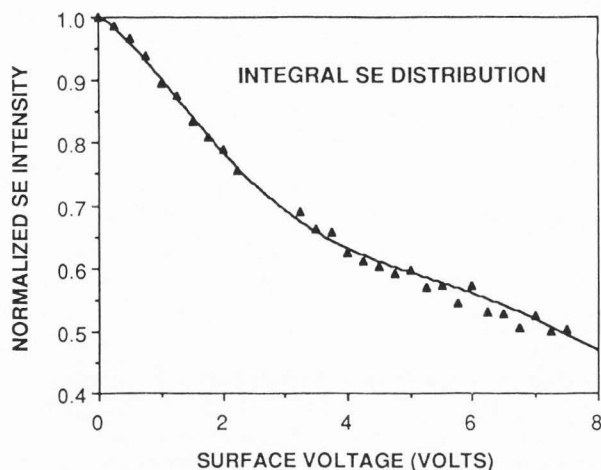


Figure 11. Integral SE distribution as measured from the peak CCVC intensity with 3.4 volt offset and best fit curve [31].

signal, from the surface potential to infinity (50 eV). When the sum of the applied and equilibrium voltages is zero, the integral SE signal is maximized. Negative surface potentials do not increase the SE signal. The peak CCVC intensity immediately after an applied transition voltage is seen in Figure 11 for a 500 eV primary electron beam [31]. This applied voltage is offset by +3.4 volts such that the maximum occurs at a surface voltage of 0.0 volts. The offset indicates an equilibrium surface voltage of 3.4 volts (which is used to find δ). This data is then used in Eq. 4 above along with the value of η given by Gorlich et al. [13]. The 3.4 volt equilibrium voltage implies that a -1 volt change on the surface would result in CCVC decay from 2.4 to 3.4 volts. The calculated decay curves and normalized data for $V(t=0) = 0.4, -0.6,$ and -1.6 volts (-3, -4, and -5 volts applied voltage changes respectively) are shown in Figure 12 (d was measured using a thin film gauge). The -0.6 and -1.6 volt curves agree reasonably well with the measured data, but the modeled 0.4 volt curve does not decay as quickly as that of the measured data. This discrepancy is probably a result of beam current drift, which can be significant at low primary beam energies and beam currents on the instrument used for this particular measurement (measured values for these data were 1.25 keV and 0.011 nA on an ETEC Autoscan SEM).

Future Research With CCVC

CCVC decay may be used to determine structure depth. The low primary beam energies required for this technique make it non-destructive when compared to the other methods. Eq. 3 above predicts that CCVC decay times should be inversely

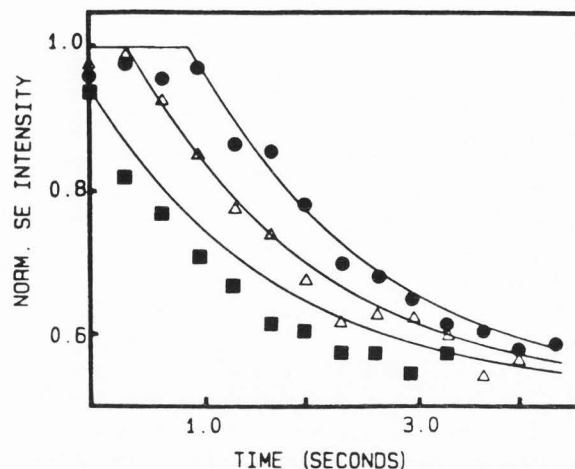


Figure 12. Calculated CCVC decay curves from experimental integral SE energy distribution and decay data for 0.4, -0.6, and -1.6 volt initial surface voltages [31].

proportional to device depth (d). Gorlich et al. have presented data which agree qualitatively with this prediction [13]. Quantitative measurements, however, are complicated by the same surface contamination which hinders CCVC modeling. To eliminate differences caused by surface contaminants, different structures on the same device with identical electron beam exposure history can be examined. Relative differences in CCVC decay data can then be compared for depth information.

The effects of different depths and dissimilar device structures (passivation over metal and passivation over silicon) can be seen in Figures 13 and 14 [31]. These images were acquired at 2.0 keV. The passivation surface approaches equilibrium potential at different rates depending on the structure below (the electrical connections to the devices are floating). This phenomenon may eliminate the need for applied voltage to measure device depth using CCVC and may therefore permit inspection of buried structures on wafers during processing.

Work is currently in progress to improve TRCCVC modeling so that voltage and depth measurements can be made from SEM-device conditions alone. However, changes in SE emission coefficients from surface contamination must be eliminated or quantified before quantitative modeling can proceed. Low energy argon plasma cleaning has proven to be a non-destructive means of removing the contamination visible in SE images and is a simple way to insure clean device surfaces initially [31]. Surface hydrocarbon contamination during beam exposure may also be reduced through use of a turbomolecular pump vacuum system rather than an oil diffusion pump. The

effects of SEM contamination can then be reduced and model deficiencies more easily recognized.

Improvement of the models for SE and BSE emission (particularly at low primary beam energies) is necessary for accurate TRCCVC measurements. Monte-Carlo methods to model the emission mechanism, which take into account low energy scattering physics, are currently under examination [31]. This as well as other methods to define SE energy distributions and BSE emission characteristics will be required for quantitative modeling.

The effects of local electric fields from nearby structures should also be examined, since they have been found to be a factor limiting resolution in static voltage contrast [40]. While the same absolute contrast difference limitations that have restricted static voltage contrast can be expected to effect TRCCVC, the change in decay times, if any, has yet to be determined.

Resistive Contrast Imaging

Resistive Contrast (absorbed current) imaging, like EBIC, uses the current produced by the electron beam/device interaction to generate an image [36]. The hardware used is identical with that for EBIC imaging, however, the physics governing image creation and the information obtained are very different for the two techniques.

As the name suggests, RCI produces an image whose contrast depends on device resistance. The basic principles governing RCI image formation are demonstrated in Figure 15. The DUT functions as a current divider, splitting the total absorbed current (I_b) between the two points shown. (The absorbed current is the difference between the incident beam current, I_b , and the total emission current, I_e .) The variation in the two path resistances, R_1 and R_2 , with primary beam position modulate the current, I_s , to form the RCI image. Smith et al. [36] have shown that the resistance ratio, R_1/R_2 , is given by:

$$\frac{R_1}{R_2} = \left(\frac{I_b}{I_s} \right) - 1 \quad (7)$$

Note that in contrast to EBIC imaging, there is no electron-hole pair charge multiplication of the current. Therefore much higher primary beam currents (20-100 nA) must be used to produce an image with RCI than with EBIC [36]. On the other hand, the primary beam need only penetrate the passivation as far as the surface metallization layer. In order to prevent electron penetration to subsurface junctions, lower beam energies are used than those needed for EBIC. Indeed,

the EBIC effect must be avoided to prevent masking of the weaker RCI signal.

One obvious application of RCI is for the detection of open circuits. Figure 16 shows a secondary and RCI image of the same device. While barely visible in the SE image, the open failure is very clearly seen using RCI. Schick has used this method to locate fragile open failures in bi-level metal structures, where the application of voltage contrast could be sufficient to "heal" the site (personal communication). RCI is also useful to view metallization patterns when the passivation surface is charged [22]. Under these conditions the SE image can be obscured, but the RCI image is unaffected. Additionally, differences between RCI images of functional and failed devices can be used to detect and locate failures such as excessive leakage currents.

Future applications of RCI will include quantitative resistance measurements. At the present, only measurements on bulk crystals have been performed [17,25]. Smith et al. showed the feasibility of measurements on IC's by using RCI on polysilicon resistors [36]. However, the effects of variations in passivation thickness and multiple current paths, especially in complicated devices, will have to be considered before quantitative measurements can be interpreted correctly.

EBIC and BSE Imaging of Semiconductors

When a beam of high energy electrons such as the primary beam in the SEM impacts on a solid sample, the primary electrons penetrate the surface, undergoing elastic and inelastic scattering events.

This results in the creation of electron-hole pairs within the sample bulk and the emission of low- and high-energy electrons and other species from the sample surface. These interactions provide information about the chemical and physical characteristics of the sample. The region of interaction between beam and sample, the interaction or excitation volume, is roughly spherical or pear-shaped [44]. The size of the interaction volume depends upon sample atomic number and weight, sample density, and beam energy. The maximum beam penetration depth, R , of the primary electron beam is an exponential function of beam energy and sample characteristics. In silicon, R may be approximated by the formula:

$$R = 0.22 E^{1.65} \quad (8)$$

where R is the maximum penetration depth in microns and E is the primary beam accelerating voltage in keV [31]. For a 30 keV beam (a typical maximum beam energy on many commonly available SEM's), R is

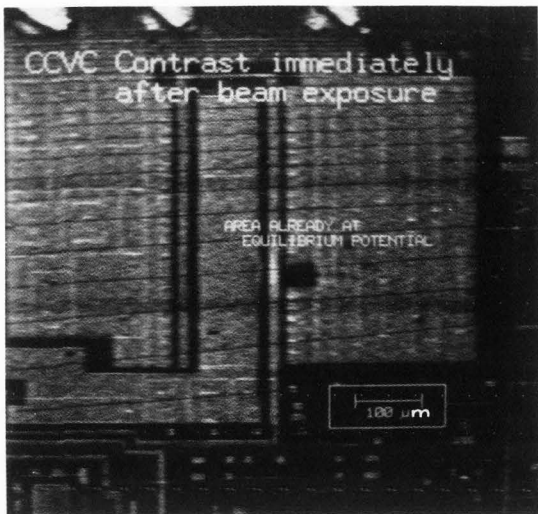


Figure 13. CCVC image of a power transistor immediately after beam exposure. The small dark square in the center had been previously examined and is at equilibrium potential [31].

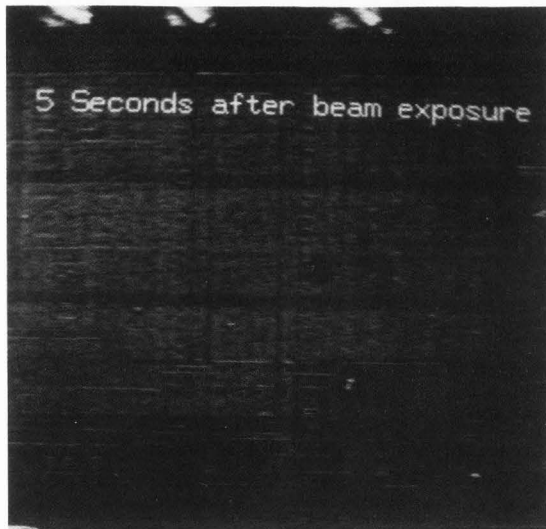


Figure 14. CCVC image of a power transistor 5 seconds after beam exposure [31].

about 6 microns. The electron beam -- sample interactions deep within the sample provide information about the internal composition and subsurface structure of the sample. This information is useful in semiconductor imaging for device depth profiling, layer thickness measurement, and detection of subsurface faults.

EBIC images have been used to characterize material parameters, detect as well as locate defects, and display the location and geometry of p-n junctions [21,30]. Digital acquisition and processing of image

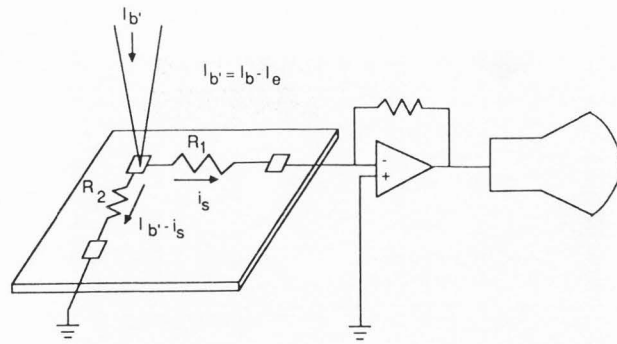


Figure 15. Experimental set for RCI experiments [37].

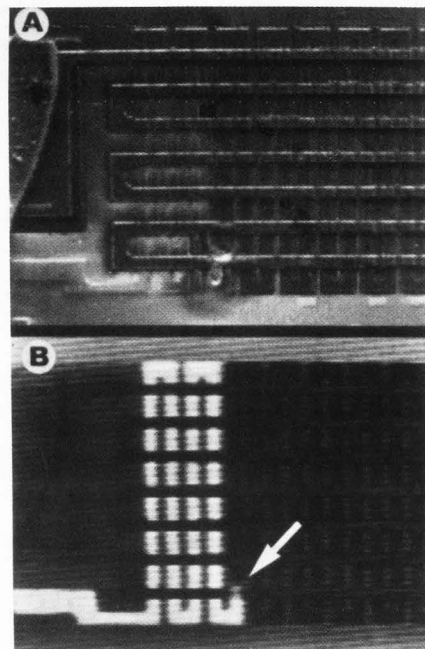


Figure 16. SE (A) and RCI (B) images of an 8-micron double metal pattern. An open-circuit failure is easily located in the RCI image (arrow) [37].

data permits quick analysis of mask misalignment as seen in Figure 17. Bresse [2] has presented an overall review of EBIC techniques and Schick [33] and Holt and Lesniak [16] have excellent reviews of current EBIC and modified EBIC techniques and applications.

There are several approaches to determining p-n junction depth with EBIC. Possin and Kirkpatrick have presented a method based on the relationship between collection probability at a p-n junction and the depth of electron hole pair generation as a function of beam energy [30]. For example, they derived the following relationship between beam

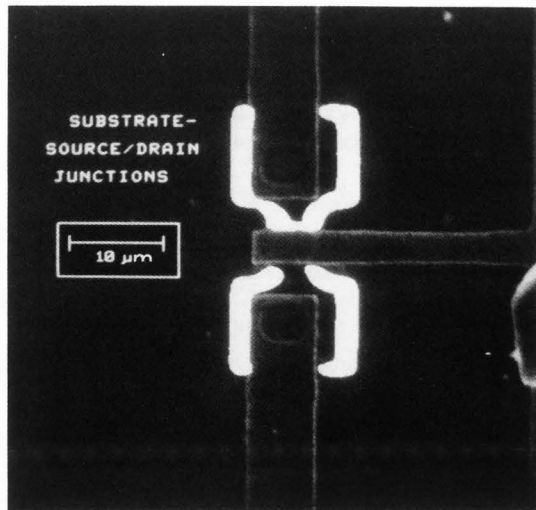


Figure 17. Combined EBIC and SE image of an FET. The asymmetry in the junction position around the metal was caused by mask misalignment [31].

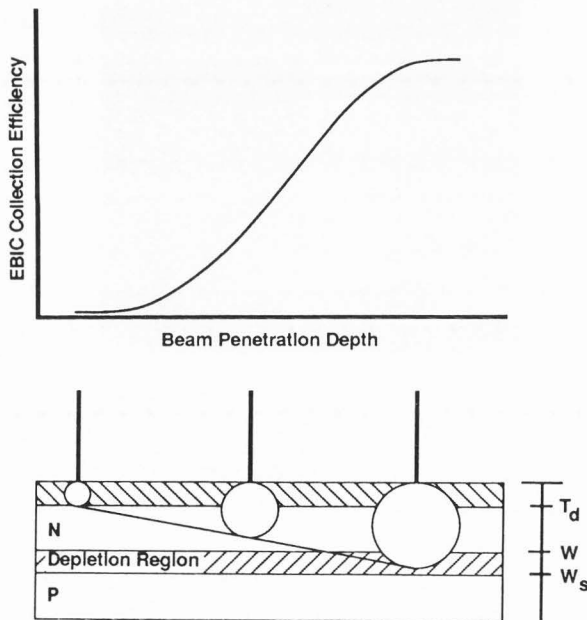


Figure 18. Schematic diagram of EBIC collection efficiency vs. beam penetration depth. Signal amplitude is proportional to the distance between the beam excitation volume and the electrically active region of the p-n junction [30].

penetration depth and charge collection efficiency in a uniformly doped diode (assuming zero bulk recombination):

$$P(z) = \begin{cases} 0 & z < T_d \\ 1 + (S_v/D)(z - T_d) & T_d < z < W \\ 1 + (S_v/D)(W - T_d) & W < z \end{cases} \quad (9)$$

In the above expression, z is the maximum beam penetration depth, T_d is the depth of the electrically inactive region above the p-n junction, W is the depth of the depletion region (measured from the surface of the device), S_v is the surface recombination velocity, and $D = (kT/q\mu)$ is the minority carrier diffusion constant in the sample material. Expressions for $P(z)$ under other conditions were also obtained. Using the proper $P(z)$, the depth of the electrically active region of the p-n junction can be determined from experimental measurement of EBIC collection efficiency as a function of beam energy (Figure 18). Chi and Gatos [3] have demonstrated a method which takes advantage of the fact that the EBIC signal has a maximum at the vertical components of a p-n junction, because of the increased area of interaction between the beam excitation volume and the depletion region. Their model predicts that electron beam excitation volumes with R greater than approximately twice the junction depth will interact with equal space charge volumes along the planar and vertical components of the p-n junction. Thus, the EBIC signal strength will be constant at all points along the p-n junction. By finding the critical beam energy at which the EBIC signal maximum disappears, the depth of the planar region of the p-n junction can be determined (Figure 19).

Backscattered electron emission (BSE) also lends itself to depth profiling if the backscattering efficiencies of the layered materials are significantly different. Detectable BSE are generated from as deep in the sample as one third to one half R , the maximum beam penetration depth, while SE escape from a depth of only 10-50 nm, depending upon the sample material. Above approximately 5 keV, BSE emission efficiency is relatively independent of primary beam energy [26,32]. This suggests that in a layered sample consisting of materials with significantly different BSE coefficients, a sharp change in the BSE signal should be observed as the beam penetrates through the upper layer into the lower layer. For example, Figures 20 & 21 show the alignment register on a Honeywell 2195F process test chip. The fabrication process used for this chip includes a thin barrier layer of a titanium/tungsten compound between the silicon and metallization layers. Titanium and tungsten have high atomic weights and consequently high backscattering efficiencies ($\eta = 0.55$).

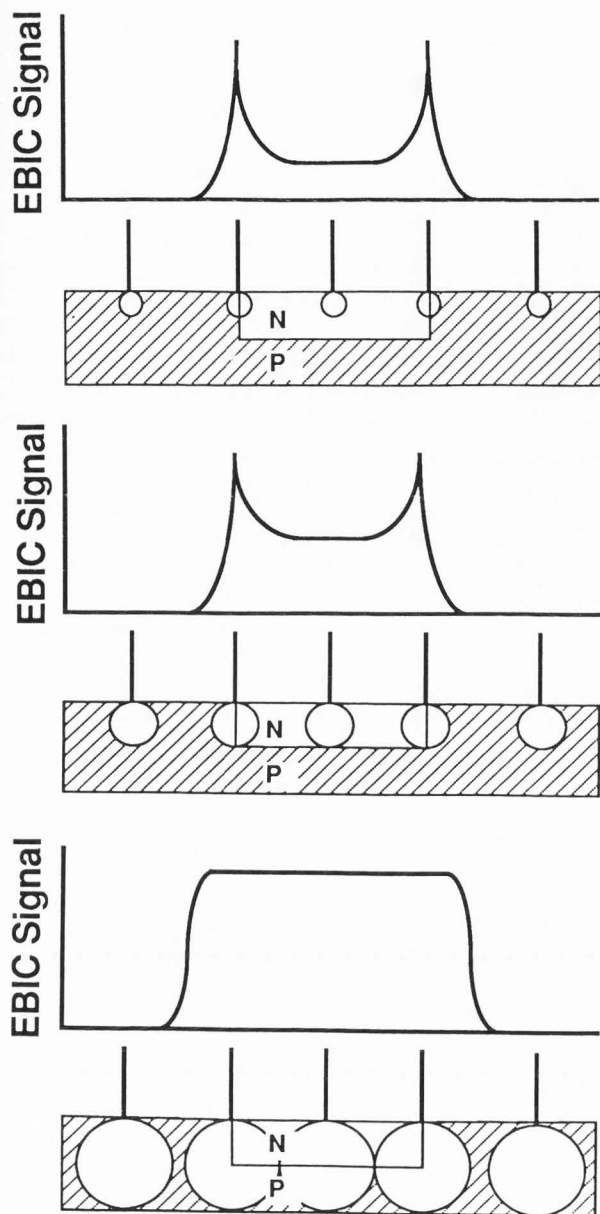


Figure 19. Schematic diagram of EBIC collection efficiency versus p-n junction geometry. Signal amplitude is proportional to the size of the region of interaction between the space charge volume and the beam excitation volume [3].

Aluminum and silicon, on the other hand, have relatively low backscattering efficiencies ($\eta = 0.2$). Figure 20 is a digital micrograph of the alignment register with a beam accelerating voltage of 5 keV and maximum penetration depth $R = 0.3$ microns. The only contrast visible in this image is due to a surface metallization layer. Figure 21 is an image of the same region of the device with the primary beam accelerating voltage increased to 20 keV ($R = 3$

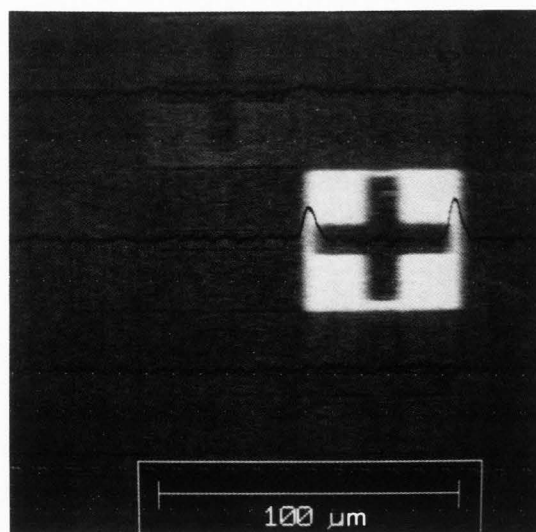


Figure 20. Digital BSE micrograph of the alignment register on a Honeywell 2195F integrated circuit. Beam accelerating voltage is 10 keV [31].

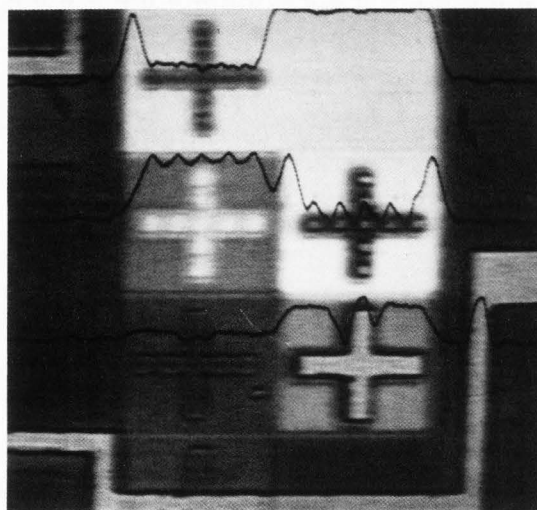


Figure 21. The same region of the device. Beam acceleration voltage is 20 keV. Bright regions correspond to buried metallization runs [31].

microns). At this voltage, the primary beam penetrates to the buried barrier layers, which show up as bright regions in the image. Work is currently in progress to develop quantitative methods for depth profiling and subsurface failure analysis using the BSE imaging mode. While this is not a low energy technique, methods such as beam blanking, windowing, and node scanning may be used to prevent or limit damage to the DUT.

Functional Testing of IC's using the SEM

Since the early 1970's, several systems have been developed with the primary purpose of performing failure analysis of integrated circuits [23,9,28,37]. IC failure analysis is extremely labor-intensive, since it requires the correlation of data from many different sources. Current SEM IC failure analysis systems can be classified as either: 1) raster-scan based imaging systems or 2) point-sampling based systems. The raster-based systems perform all data processing in a homogeneous manner on entire images. For point-sampling systems, data is acquired and processed from a limited number of areas of interest (or nodes). This data is usually displayed by means of a set of waveforms.

One of the major drawbacks of raster-based systems is the enormous amount of data which must be acquired, processed and stored. A typical image size is 512×512 picture elements (or pixels) where each pixel is digitized to a resolution of 8 bits, which consumes 0.25 Mbytes of storage. This value, however, is not the amount of data required to actually perform failure analysis on the DUT. Assume that the DUT can be digitized with sufficient resolution and stored in one 512×512 pixel image. If the number of possible states in which a fault can occur is on the order of 2000 (not unreasonable for a typical VLSI device), then the raster-based system must acquire and process around 1 GByte of VC information. This is compounded if the DUT cannot be digitized with sufficient resolution in one 512×512 pixel image. In 1985, Oxford and Propst observed that these problems can be reduced by an order of magnitude by noting that much of the area on a typical VLSI device is covered by metallization and not by active devices [28]. Thus, data acquisition should be confined to only those areas (or nodes). This technique is a hybrid between raster-based imaging and point sampling, since each of the individual areas of interest may have an arbitrary shape. One advantage of this approach over point-sampling is that the use of a raster format for the areas of interest allows the application of filtering and statistical techniques in the spatial domain as well as in the temporal domain.

All of the systems described above, however, share two general shortcomings: 1) each of the systems is limited to a single data acquisition mode (such as VC imaging) and 2) there is no link between the Computer-Aided Design (CAD) data and the failure analysis system. The first problem prevents the failure analysis system from determining any information other than which device (or set of devices) is malfunctioning. More specific

information, such as mask misalignment can be easily determined using EBIC imaging, and should be included in a complete failure analysis system. In 1986, Kuji et. al. described a system which addressed the second of these shortcomings [20]. The system described provides automatic identification of incorrect voltages by a comparison of the DUT with the CAD data. Thus, a great portion of the failure analysis task has been automated. However, this system is entirely raster-based (with the associated problems described earlier), and is also limited to VC data acquisition only. Before truly automated SEM-based IC failure analysis systems can become reality, the problems outlined above will have to be resolved.

The automation of at least part of the integrated circuit failure analysis process is a goal which has been discussed since the 1970's. Early SEM IC analysis systems used computers to control the primary beam scanning position only. The image data was processed in analog form by the SEM hardware. This processing was generally limited to video frame subtraction, addition and averaging. In 1976, Oron and Gilbert described a system which used a computer not to control the primary beam position but to digitize and store VC image data from the DUT [27]. Subsequently, numerous systems have been described in which a computer performs both functions. Systems such as that described by Walter et. al. [41], were able to locate individual conductors in an IC and acquire voltage waveform data from them. However, computer control of the primary beam position alone is not sufficient to ensure repeatability of VC measurements. Another requirement which must be met for an automatic SEM IC analysis system is the computer-control of microscope operating parameters. These parameters include (but should not be limited to) working distance, magnification, and primary beam spot size. In order to produce repeatable quantitative VC measurements, these parameters must be constant from one measurement to the next. Several SEM manufacturers now include the means for automatically maintaining focus (working distance) and stigmation, but most current SEM IC analysis systems rely on the operator to ensure that the operating parameters are consistent from one measurement to the next.

Conclusions

At present, the dominant IC fabrication process is based on the MOS technology, since it provides the highest density for commercially available devices. However, the operating characteristics of an MOS device are extremely sensitive to traps in the gate oxide regions. These traps can result from the

penetration of high-energy electrons, such as those of an SEM primary beam, into the gate area of the DUT. Thus, investigations of the effects of high energy electrons (such as a primary electron beam) passing through MOS devices are of great interest to current researchers.

Another potential source of damage to the IC structure are the X-rays created by the high-energy primary electrons. For this reason, voltage contrast measurements on MOS devices are usually confined to low (under 1 keV) primary beam energies. Other factors also affect the choice of the proper accelerating voltage, such as the tendency of the DUT to accumulate charge (either positive or negative, depending on the accelerating voltage). In order to study the operation of the typical MOS device, both of these effects must be minimized to duplicate as closely as possible the normal operating conditions of the DUT.

Low-voltage applications of the SEM offer measurement tools for the evolving semiconductor industry. Mechanical wafer probing has gone from difficult to impossible at submicron device dimensions. E-beam probing methods are already available to assume the responsibility for the future. Waveform stroboscopic systems are currently available, such as the Applied Beam Technologies ABT IL-200, which allow submicron and subnanosecond voltage probe measurements.

The next generation of SEM systems will have the opportunity to combine in-line physical and electrical device parameter analysis and dynamic voltage probing along with image processing and storage. This integrated with Automated Test Equipment and cassette loading will provide a suitable test and evaluation environment for submicron technology.

Acknowledgement

The authors would like to thank Mr. Ron Kalin (Honeywell Solid State Electronics Div., Plymouth, MN) for supplying the test devices used in this research. The authors' research (including some of the work described in this manuscript) is supported by the Semiconductor Research Corporation under contract 86-07-083.

References

- [1] Balk LJ, Feuerbaum HP, Kubalek E, Menzel E. (1976). Quantitative Voltage Contrast at High Frequencies in the SEM. *Scanning Electron Microsc.* 1976; I:615-624.
- [2] Bresse JF. (1982). Quantitative Investigations in Semiconductor Devices by Electron Beam Induced Current Mode: A Review. *Scanning Electron Microsc.* 1982; IV:1487-1500.
- [3] Chi J, Gatos HC. (1977). Nondestructive Determination of the Depth of Planar p-n Junctions by Scanning Electron Microscopy. *IEEE Trans. Elect. Dev.* ED-24, 1366-1367.
- [4] Cocito M, Soldani D. (1981). Evaluation of the Performance of an Electron Beam Testing System based on Commercially Available Subsystems. *Scanning Electron Microsc.* 1981; I: 45-54.
- [5] Cole EI, Bagnell CR, DiBianca FA, Johnson D, Oxford W, Smith C, Propst RH. (1986). Time-resolved Capacitive Coupling Voltage Contrast--A New Voltage Measurement Technique for Passivated Devices. *Applied Physics Letters.* 48(9). 599-600.
- [6] Dentges D, Gorlich S, Kubalek E. (1986). Computer simulation and Experimental Performance Data for an Electron Spectrometer for Electron Beam Testing of Integrated Circuits. *Scanning Electron Microsc.* 1986; I: 45-56.
- [7] DiBianca FA, Johnson DG, Bagnell CR, Cole EI, Oxford WV, Propst RH, Smith CS. (1986). Data Acquisition and Processing Techniques for Voltage Contrast Measurements. *Scanning Electron Microsc.* 1986; I: 57-64.
- [8] Driver MC. (1969). A Spherically Symmetrical Detector for the Scanning Electron Microscope. *Scanning Electron Microsc.* 1969; I: 403-413.
- [9] Feuerbaum HP, Hernaut K. (1978). Application of Electron-beam measuring techniques for the verification of computer simulation of large-scale integrated circuits. *Scanning Electron Microsc.* 1978; I: 795-800.
- [10] Feuerbaum HP. (1979). VLSI Testing Using the Electron Probe. *Scanning Electron Microsc.* 1979; I: 285-296.
- [11] Fujioka H, Tsujitake M, Ura K. (1982). Voltage Contrast Isolation by frame-by-frame Subtraction in the Scanning Electron Microscope. *Scanning Electron Microsc.* 1982; III: 1053-1060.
- [12] Fujioka H, Nakame K, Ura K. (1983). Voltage Measurements on Passivated Electrodes with the Scanning Electron Microscope. *Scanning Electron Microsc.* 1983; III: 1157-1162.
- [13] Gorlich S, Herrmann KD, Kubalek E. (1985). Proceedings of the Microcircuit Engineering 84 Conference. Basic Investigations of Capacitive Coupling Voltage Contrast. Academic Press, London. 451-460.
- [14] Gorlich S, Kubalek E. (1985). Electron Beam

- Induced Damage on Passivated Metal Oxide Semiconductor. *Scanning Electron Microsc.* 1985; I: 87-95.
- [15] Halbritter J. (1983). Resonant Emission of Secondary Electrons. *Scanning Electron Microsc.* 1983; II: 511-519.
- [16] Holt DB, Lesniak M. (1985). Recent Developments in Electrical Microcharacterization Using the Charge Collection Mode of the Scanning Electron Microscope. *Scanning Electron Microsc.* 1985; I:67-86.
- [17] Kamm JD, Muller R. (1977). Two Dimensional Plotting of Semiconductor Resistivity by Scanning Electron Microscope. *Solid-State Electronics*, 20, 105-110.
- [18] Knoll M. (1935). Static Potential and Secondary emission of bodies under electron irradiation. *Z. Tech. Phys.* 11, 467-475.
- [19] Kotorman L. (1980). Non-Charging Electron Beam Pulse Prober on FET Wafers. *Scanning Electron Microsc.* 1980; IV: 77-84.
- [20] Kuji N, Tamama T, Nagatani M. (1986). FINDER: A CAD System-Based Electron Beam Tester for Fault Diagnosis of VLSI Circuits. *IEEE Transactions on Computer-Aided Design*. Vol. CAD-5. No. 2. April 1986; 313-319.
- [21] Leamy HJ, Kimerling LC, Ferris SD. (1978). Electron Beam Induced Current. *Scanning Electron Microsc.* 1978; I:717-725.
- [22] Maussion M. (1985). High Resolution Scanning Electron Microscopy With Absorbed Current at Low Intensity Primary Beams. *J. Phys. E.* 18(1). 1-13.
- [23] May TC, Scott GL, Meieran ES, Winer P, Rao VR. (1984). Dynamic Fault Imaging of VLSI Random Logic Devices. *Proceedings of the 22nd Annual Reliability Physics Symposium.* (IEEE), 1984; 95-108.
- [24] Menzel KE, Kubalek E. (1983). Fundamentals of Electron Beam Testing of Integrated Circuits. *Scanning*, 5, 103-122.
- [25] Munakata C. (1966). Detection of Resistivity Striations in a Ge Crystal with an Electron Beam. *Japan. J. Appl. Phys.*, 5, 336.
- [26] Niedrig H. (1982). Electron Backscattering from Thin Films. *J. Appl. Phys* 53(4), R15-R43.
- [27] Oron M, Gilbert D. (1976). Combined Scanning Electron Microscope - minicomputer system for digital image processing. *Scanning Electron Microsc.* 1976; I: 121-128.
- [28] Oxford WV, Propst RH. (1985). Efficient Failure Analysis of Integrated Circuits using Scanning Electron Microscopy. *IEEE Transactions on Reliability*. Vol. R-34. No. 5, Dec. 1985; 410-417.
- [29] Plies E, Otto J. (1985). Voltage measurements inside Integrated Circuits using Mechanical and Electron Probes. *Scanning Electron Microsc.* 1985; IV: 1491-1500.
- [30] Possin GE, Kirkpatrick CG. (1979). Electron Beam Depth Profiling in Semiconductors. *Scanning Electron Microsc.* 1979;I:245-254.
- [31] Propst RH, Bagnell CR, DiBianca FA, Cole E, Davies B, Johnson D, Lipkin L, Oxford W, Neacsu A, Roy S, Smith C, Vance J. Quarterly and Annual Reports to the SRC, Contract No. 83-01-025, 9/83-9/86.
- [32] Reimer L. (1985). *Scanning Electron Microscopy*, Springer-Verlag, Berlin. 45. 135-139.
- [33] Schick JD. (1985). Advances in Electron-Beam-Induced-Current Analysis of Integrated Circuits. *Scanning Electron Microsc.* 1985; I:55-66.
- [34] Seah MP. (1969). Slow Electron Scattering From Metals, I. *Surface Science*, 17. 132-160.
- [35] Seiler H. (1983). Secondary Electron Emission in the Scanning Electron Microscope. *J. Appl. Phys.* 54(11). R1-R18.
- [36] Smith CA, Bagnell CR, DiBianca FA, Cole EI, Oxford WV, Propst RH. (1986). Resistive Contrast Imaging: A New SEM Mode For Failure Analysis. *IEEE Transactions on Electron Devices*. ED-33, No. 2. 282-285.
- [37] Stivers AR, Ferguson DC. (1986). Fault Contrast: A new voltage contrast VLSI diagnosis technique. *Proceedings of the 24th Annual Reliability Physics Symposium.*(IEEE), 1986; 109-114.
- [38] Taylor DM. (1978). The effect of Passivation on the Observation of Voltage Contrast in the Scanning Electron Microscope. *J. Phys. D*, 11. 2443-2454.
- [39] Ura K, Fujioka H, Nakamae K, Ishisaka M. (1982). Stroboscopic Observation of Passivated Microprocessor Chips by Scanning Electron Microscopy. *Scanning Electron Microsc.* 1982; III: 1061-1068.
- [40] Ura K, Fujioka H, Nakamae K. (1984). Reduction of Local Field Effect on Voltage Contrast. *Scanning Electron Microsc.* 1984; III: 1075-1080.
- [41] Walter MJ, Eldering CA, Krevis KM, Haberer JR. (1982). Internal Node Testing by Tester Aided Voltage Contrast. *Proc. of International Symposium for Testing and Failure Analysis (ISTFA)*. 1982; 156-161.
- [42] Wells OC, Bremer CG. (1968). Voltage Contrast Measurement in the scanning electron microscope. *J. Phys. E. Sci. Instr. Series 2*, 1968; 902-906.

- [43] Wells OC. (1969). An Irradiation Effect in Thermally Grown SiO₂. Appl. Physics Letters. 14. 5-6.
- [44] Wells OC. (1974). Scanning Electron Microscopy. McGraw Hill, New York. 180-207.

Discussion With Reviewers

J.R. Beall: What is the practical limit of resistance resolution for RCI with "today's" instrumentation? Is it practical to use RCI on complex circuits with 1) the required beam current hence larger electron beam probe size and, 2) the limitation of intercepting (imaging) the induced beam current injected into complex circuits (due to limited circuit node access)?

Authors: The precision of the resistance value measured will be dependent upon complex current paths which cannot be easily modeled. Only isolated resistors could be used for resistance calibration (which we have not done), and even then the SE and BSE fractions as well as leakage through the isolation stage must be considered. The method is most useful to identify breaks or shorts in metallizations and for comparing functional to failed devices ([36]). The large beam currents required do limit spatial resolution to some extent. Still, better than 1.0 micron resolution is easily obtainable, using a primary beam current of tens of nA, (which gives us an RCI current on the same order of magnitude). We can use such small RCI currents due to the large gain of the current-to-voltage converter used for RCI and EBIC experiments (1.0 nanoamp to 1.0 volt). In order to produce this large a gain without limiting bandwidth, however, a multi-stage signal amplifier must be employed.

Complex gate-array devices have been examined without difficulty. These contain circuit elements which are far from an access node displaying resistive contrast. The major problem with complicated devices is the amount of memory required to store and process images of the entire device, not the lack of RCI information available from the interior of the device.

J.R. Beall: In TRCCVC you describe the measurement of negative voltage transitions, is this measurement method less sensitive to positive voltage transitions? How does TRCCVC perform in the 0.1 to 1.0 volt signal level?

L. Kotorman: The CCVC signal could be caused by a negative or positive voltage transition, and instead of causing more SE's to escape, would not a positive transition cause a decrease rather in the rate of secondaries before an equilibrium potential would be reached again?

Authors: Positive voltage transitions have no saturation region like negative changes and decay more quickly than a negative change of the same magnitude. These differences in decay times are explained by the model of Gorlich et al. [13]. The loss of temporal resolution will reduce the voltage resolution obtainable with TRCCVC and we are currently experimenting with positive transitions to determine this resolution. Since we originally videotaped our data and later digitized the signal, the onset of the TRCCVC decay had to have a large enough contrast change to be seen visually. The frame digitizer could then be synchronized to device operation. The smallest voltage change that could be easily identified visually was 0.75 volts, as shown in Table 1. Smaller voltage transitions could be acquired if the applied bias and frame digitizer were driven by the same computer. At these smaller voltages there would be no saturation time, and so temporal resolution would be reduced. The decay times would still be longer for larger voltage transitions below the saturation level.

J.R. Beall: In Table 1, how were the voltage contrast levels interpreted to determine the voltage error?

Authors: The decay times to the target intensity for various applied voltages were linearly fitted to the applied bias (Figure 8). The error was then determined by the difference between the actual applied bias and that predicted by the linear calibration curve.

J.R. Beall: What is the maximum signal frequency that can be measured using TRCCVC?

L. Kotorman: To relate the "CCVC" storage time to voltage levels appears to be a useful technique in certain conditions. However, the CCVC is very often used to measure dynamic waveforms where the device transitions are in the nanosecond or sub-nanosecond range and the repetition or cycle times are perhaps in the hundreds of nanoseconds. Would the authors envision any utilization under these conditions please?

Authors: The maximum frequency available using standard videotape methods is 30 Hz (30 video frames per second). Higher frequencies should be possible using beam blanking and a faster signal digitizer. Higher incident electron fluxes would also be required for the CCVC signal to decay over the required period. Complete decay to equilibrium is required for the TRCCVC method described above.

L. Kotorman: Would it be possible to rename the so-called "TRCCVC", since "time resolved voltage contrast" generally refer to high speed dynamic waveforms? Several authors did refer to the decay time of the CCVC such as: "storage time". Would you think perhaps this label would be more appropriate?

Authors: We feel that since the TRCCVC method described is based upon the temporal resolution of the CCVC decay for quantitative measurement, the "time resolved" designation is appropriate.

L. Kotorman: Could you please comment on the procedures which were used to neutralize the surface before the measurements were taken?

Authors: The surface was brought to equilibrium by scanning over the device until no change in contrast was observed for 5 seconds. The transition potentials used for CCVC data were square waves with periods long enough for the surface to re-establish equilibrium for 3 seconds before further voltage change.

L. Kotorman: It is stated in the text that: "the secondaries with energies greater than the surface potential will escape". What cautions were observed to eliminate or escape surface barrier potential conditions? Would you think that the decay time constants would vary for any other reason in relation to the physical size of the nodes being measured?

Authors: The secondary electrons we include in the integral SE distribution are those which would normally escape the surface barrier with no surface charge build up or applied bias. The "secondaries" to which we refer are those SE which have sufficient energy to overcome the surface barrier potential and any surface voltage, both equilibrium and applied. The decay mechanism we have shown is based on a simple parallel plate capacitor model, and if the nodes are small enough that edge effects are significant, the decay times will vary. Thus far, the TRCCVC technique has been tested using 1.25 micron polysilicon test

conductors under 0.350 microns of thermal oxide, and uniform decay was observed across the width of the structure.

L. Kotorman: Concerning the discrepancy on the 0.4V curve which you say was probably caused by "beam current drift". What do you think is the major cause of the unstable beam current?

Authors: At primary beam energies below 10 keV, the high voltage power supply of the ETEC Autoscan SEM used for these experiments is unstable and will cause fluctuations in the beam current. Over a 10 minute period at 1.25 keV we have observed variations of 20 percent. Newer microscopes, designed for operation at beam energies of 1.0 keV and below, will reduce this problem.

L. Kotorman: In your experience please what type of surfaces exhibit the worst of contamination problems? Do you think that voltage levels on the surface may play any role in the rate of contamination?

Authors: Surfaces examined without any type of cleaning, such as low energy argon plasma etching, are the most prone to contamination. Even with cleaning, changes in SE emission are observed after several minutes of exposure to a 10 keV primary electron beam. Using a turbomolecular pump instead of an oil diffusion pump, outgassing the sample for 24 hours before beam exposure, and using lower primary beam energies does reduce the rate of contamination build up. Our observations have indicated no difference in surface contamination rates over biased and unbiased regions.